Oxide Ion Conductors

DOI: 10.1002/anie.201106111

Remarkably High Oxide Ion Conductivity at Low Temperature in an Ordered Fluorite-Type Superstructure**

*Xiaojun Kuang, Julia L. Payne, Mark R. Johnson, and Ivana Radosavljevic Evans**

Oxide ion conductors are technologically important materials because of their potential applications in oxygen sensors and pumps, as dense membranes for oxygen permeation, catalysts, and as electrolytes for solid oxide fuel cells (SOFCs).[1–4] To be efficient in various applications, candidate materials should possess a conductivity of at least $10^{-2}\,S\,cm^{-1}$ at device-operating temperatures; currently commercially used yttria-stabilized zirconia (YSZ) reaches this target at 700 °C.[1] Given the drive towards lowering device-operating temperatures, there is a strong impetus and a great challenge for materials chemists to develop materials with enhanced ionic mobility and superior low-temperature oxide ion conductivity.[5,6] A better understanding of generic structural features and pathways which facilitate ionic mobility at lower temperature is a key step in reaching this goal.

Here we report a remarkably high oxide ion conductivity at low temperatures (300–500 °C) in an ordered pseudo-cubic $3\times3\times3$ δ-Bi_2O_3 superstructure with composition $Bi_{1-x}V_xO_{1.5+x}$ ($x=0.087$ and 0.095). Its conductivity is the highest we know of in a singly substituted δ-Bi_2O_3-based material and comparable to the unstable $Bi_{0.85}Pr_{0.105}V_{0.045}O_{1.545}$[7] and $Bi_{12.5}La_{1.5}ReO_{24.5}$ on their first use, that is, before their conversion into a stable tetragonal form and an associated drop of conductivity of almost two orders of magnitude.[8,9] By contrast and unusually, our materials crystallize as stable ordered superstructures, and do not undergo phase transitions to lower symmetry and lower conductivity polymorphs. Our ab initio molecular dynamics (AIMD) simulations reveal the structural features and mechanisms which facilitate the high oxide ion mobility at low temperatures, and provide conceptual insight readily applicable to other materials and structure types.

The high-temperature cubic fluorite-type bismuth oxide, δ-Bi_2O_3, with intrinsic oxygen vacancies, shows the highest oxide ion conductivity measured in any material (around $1\,S\,cm^{-1}$ at 750 °C);[10] however, it is only thermodynamically stable in the narrow range between 730 and 824 °C.[11] There has been considerable interest in stabilizing the highly conducting δ-Bi_2O_3 phase by isovalent or aliovalent cation substitution to preserve oxide ion conductivity at lower temperatures. For example, 20 % substitution of Er into Bi_2O_3 results in oxide ion conductivity of $2\times10^{-2}\,S\,cm^{-1}$ at 500 °C and $0.4\,S\,cm^{-1}$ at 700 °C.[12] Double cation substitution has yielded even higher conductivities at low temperatures (300–500 °C); the best examples include Dy-W,[13] Pr-V,[7] and the recently reported La-Re[8] co-substitutions. On first use, $Bi_{0.85}Pr_{0.105}V_{0.045}O_{1.545}$[7] and $Bi_{12.5}La_{1.5}ReO_{24.5}$[8] show the highest oxide ion conductivity among the doped δ-Bi_2O_3 materials, with $\sigma\approx10^{-3}$–$10^{-2}\,S\,cm^{-1}$ at 300–400 °C, approaching the Cu-doped layered $Bi_2VO_{5.5}$ (BICUVOX), which itself has the disadvantage of two-dimensional, anisotropic conductivity. Although the relative chemical instability of Bi oxides under reducing conditions has so far hampered their applications in SOFCs, the use of bilayer electrolytes can overcome this issue.[14] In addition to high oxide ion conductivity, bismuth-based oxides show electrocatalytic activity and therefore also have great potential for applications in electrochemical oxygen separation.[15,16]

A common structural feature in the best δ-Bi_2O_3-based oxide ion conductors reported so far is that doping stabilizes simple cubic structures with $a\approx$ 5.5 Å and space group $Fm\bar{3}m$.[7–8,13] By comparison, doped δ-Bi_2O_3 materials which possess long-range superstructures usually have lower conductivities.[17–19] Simple cubic doped materials, however, are often only metastable and convert to lower symmetry forms with significantly lower conductivities, which is a major obstacle to their practical use.

Initial X-ray and electron diffraction studies of the $3\times3\times3$ fluorite superstructures in the Bi_2O_3-V_2O_5 system carried out by Zhou,[20] suggested the existence of a phase with composition $Bi_{18}V_2O_{32}$ ($Bi_{1-x}V_xO_{1.5+x}$ with $x=0.100$); the closely related $Bi_{16}V_2O_{29}$ ($x=0.111$) was also found to be a $3\times3\times3$ fluorite supercell, but distinguishable from $Bi_{18}V_2O_{32}$ based on peak positions in its diffraction pattern. In our syntheses (see Methods in ESI), single-phase materials were formed for compositions with $x=0.087$ and 0.095 ($Bi_{0.913}V_{0.087}O_{1.587}$ and $Bi_{0.905}V_{0.095}O_{1.595}$), by firing the starting oxides at 825 °C for 12 h, after initial calcinations at 700, 750, and 800 °C (for 12 h at each temperature with intermediate grinding); we will occasionally refer to these two very similar compositions jointly as "$Bi_{18}V_2O_{32}$". $Bi_{16}V_2O_{29}$ started appearing as a second phase for $0.095<x<0.100$ and V-doped γ-Bi_2O_3 was present for $0.074<x<0.083$ (see Figure S1 in the Supporting Information).

Impedance measurements on $Bi_{0.905}V_{0.095}O_{1.595}$ and $Bi_{0.913}V_{0.087}O_{1.587}$ (Figure 1) were carried out on heating to

[*] X. Kuang, J. L. Payne, I. Radosavljevic Evans
Department of Chemistry, University of Durham
Science Site, Durham DH1 3LE (UK)
E-mail: ivana.radosavljevic@durham.ac.uk
M. R. Johnson
Institut Laue Langevin
38042 Grenoble (France)

[**] Financial support was provided by the EPSRC through grant EP/F030371. J.L.P. thanks the Durham University for a PhD studentship. The authors thank the ILL for computational facilities and Didier Richard and Eric Pellergrini for recent developments in LAMP and nMoldyn codes.

Supporting information for this article is available on the WWW under http://dx.doi.org/10.1002/anie.201106111.

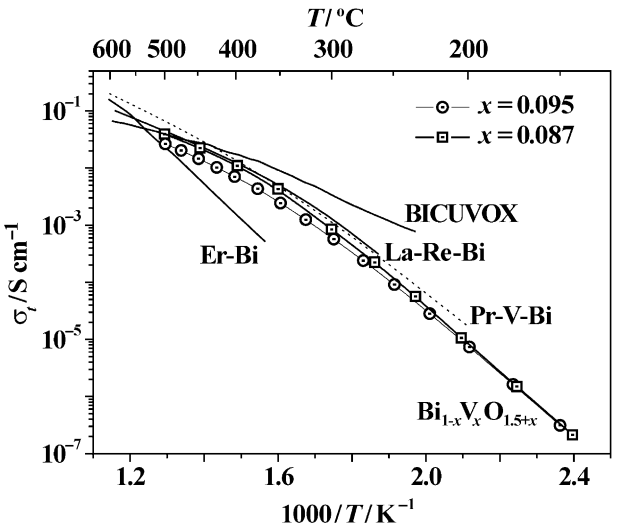

Figure 1. Ionic conductivity of $Bi_{1-x}V_xO_{1.5+x}$ with $x = 0.095$ and 0.087. The plot of total conductivity for $Bi_{0.905}V_{0.095}O_{1.595}$ (open circles) and $Bi_{0.913}V_{0.087}O_{1.587}$ (open squares) in comparison with $Bi_{0.85}Pr_{0.105}V_{0.045}O_{1.545}$[7] (Pr-V-Bi), $Bi_{12.5}La_{1.5}ReO_{24.5}$[8] (La-Re-Bi), $Bi_{0.8}Er_{0.2}O_{1.5}$(Er-Bi),[12] and $Bi_2V_{0.9}Cu_{0.1}O_{5.35}$ (BICUVOX).[21]

500 °C and on cooling back to room temperature. The complex impedance data (see Figure S2 in the Supporting Information) comprise a single semicircular arc from the bulk response and a Warburg-type electrode response below 350 °C, with a large low-frequency (< 10 Hz) capacitance of 10^{-7}–10^{-6} F cm^{-1} (> 200 °C); these observations are indicative of ionic conduction. No significant grain boundary contribution was detected in the impedance data over the measured temperature region. Three cycles of impedance measurements on heating to 500 °C and cooling back to room temperature were performed, with approximately an hour spent at each measurement point, and completely reproducible measurements with no deterioration of conductivity were obtained (see Figure S3 in the Supporting Information).

Figure 1 shows the plots of the total conductivities of our two "$Bi_{18}V_2O_{32}$" materials ($Bi_{0.905}V_{0.095}O_{1.595}$ and $Bi_{0.913}V_{0.087}O_{1.587}$), which show a gradual change of activation energies, from 1.1 eV in the low-temperature region (150–300 °C) to 0.68 eV in the high-temperature region (350–500 °C). In the temperature region from 300 to 500 °C, $Bi_{0.905}V_{0.095}O_{1.595}$ shows a conductivity of 5.7×10^{-4}–2.6×10^{-2} S cm^{-1}, whereas $Bi_{0.913}V_{0.087}O_{1.587}$ shows an even higher conductivity of 8.5×10^{-4}–3.9×10^{-2} S cm^{-1}. Data displayed in Figure 1 show that the conductivities of these materials compare favorably with the best fluorite-type low- and intermediate-temperature oxide ion conductors reported in the literature so far. Between 300 and 400 °C, $Bi_{0.905}V_{0.095}O_{1.595}$ and $Bi_{0.913}V_{0.087}O_{1.587}$ show only marginally lower conductivity than the Pr-V[7] and La-Re[8] doped δ-Bi_2O_3. From 400 to 500 °C, the conductivity of $Bi_{0.913}V_{0.087}O_{1.587}$ ($x = 0.087$) is nearly identical to that of the La-Re doubly substituted δ-Bi_2O_3 material and the layered BIMEVOX phase $Bi_2V_{0.9}Cu_{0.1}O_{5.35}$ (BICUVOX).[21] In comparison with $Bi_{0.8}Er_{0.2}O_{1.5}$,[12] the best singly substituted δ-Bi_2O_3-based material reported until now, $Bi_{0.905}V_{0.095}O_{1.595}$ and $Bi_{0.913}V_{0.087}O_{1.587}$ show significantly better performance; at 400 °C, the conductivities of our materials are an order of magnitude higher.

The conductivity we observed for $Bi_{0.905}V_{0.095}O_{1.595}$ and $Bi_{0.913}V_{0.087}O_{1.587}$ is significantly higher than that reported by Takahashi et al.[22] for the closely related composition $Bi_{0.91}V_{0.09}O_{1.59}$ (10^{-3} S cm^{-1} at 500 °C vs. 4×10^{-2} S cm^{-1}); Takahashi et al.[22] also performed electromotive force (EMF) measurements and reported a transference number $\tau = 0.96$, showing predominant ionic conductivity in this material. We believe this apparent discrepancy in conductivity values can be ascribed to the decomposition of $Bi_{0.91}V_{0.09}O_{1.59}$ to the less conducting $Bi_{16}V_2O_{29}$ and V-doped γ-Bi_2O_3[23] in their work,[22] since they performed the measurements through an instability range (500–800 °C) identified in our study and discussed below. Our own measurements of the conductivity of $Bi_{0.905}V_{0.095}O_{1.595}$ on slow cooling from 800 °C gave low values which agree with those reported by Takahashi et al.[22] (10^{-5}–10^{-3} S cm^{-1} in the range of 300–500 °C, see Figure S4 in the Supporting Information). The phase content of the pellet after this impedance measurement was determined by XRD, and clearly showed partial decomposition to $Bi_{16}V_2O_{29}$ and V-doped γ-Bi_2O_3 (see Figure S5 in the Supporting Information).

Variable temperature in situ X-ray diffraction experiments (shown in detail in the Supporting Information), performed to assess the high-temperature stability and structural behavior of $Bi_{0.905}V_{0.095}O_{1.595}$ and $Bi_{0.913}V_{0.087}O_{1.587}$, suggest that they are indefinitely stable below 450 and above 825 °C. Between these two temperatures, gradual decomposition to $Bi_{16}V_2O_{29}$ and V-doped γ-Bi_2O_3 occurs, although the "$Bi_{18}V_2O_{32}$" material remains the majority phase; for example, at 550 °C (after a total of around 36 h of heating at 400, 450, and 500 °C), "$Bi_{18}V_2O_{32}$" still comprises > 90 % of the sample, as shown by quantitative variable temperature PXRD data analysis. At 825 °C, the original "$Bi_{18}V_2O_{32}$" single phase is fully reformed, and more crystalline, as evidence by sharper diffraction peaks (see Figures S6 and S7 in the Supporting Information). A similar stability gap has also been observed for the interstitial oxide ion conductor $La_{1+x}Sr_{1-x}Ga_3O_{7+0.5x}$.[24] Thermal expansion of our materials is linear and essentially isotropic from ambient temperature to 500 °C ($\alpha_l = 1.56\times10^{-5}$ K^{-1} over this range, see Figure S8 in the Supporting Information).

Ab initio molecular dynamics (AIMD) simulations are a powerful computational tool for elucidation of oxide ion migration mechanisms, and we have previously successfully used this approach to show the conductivity based on vacancy hopping in fluorite-related bismuth-lanthanum oxide, $Bi_8La_{10}O_{27}$.[18] In the present study, our aim was to determine the roles of the constituent structural building blocks (OBi_4 fluorite-like slabs and isolated VO_4 groups, see Figure S9 in the Supporting Information) in O^{2-} migration. Full details of the starting structural model and the AIMD procedures are given in the Supporting Information.

Figure 2 shows the volumes visited by oxide ions (represented by white displacement clouds) during the course of MD simulations at 473 and 873 K, and illustrates three distinct types of typical O^{2-} exchange and migration process-

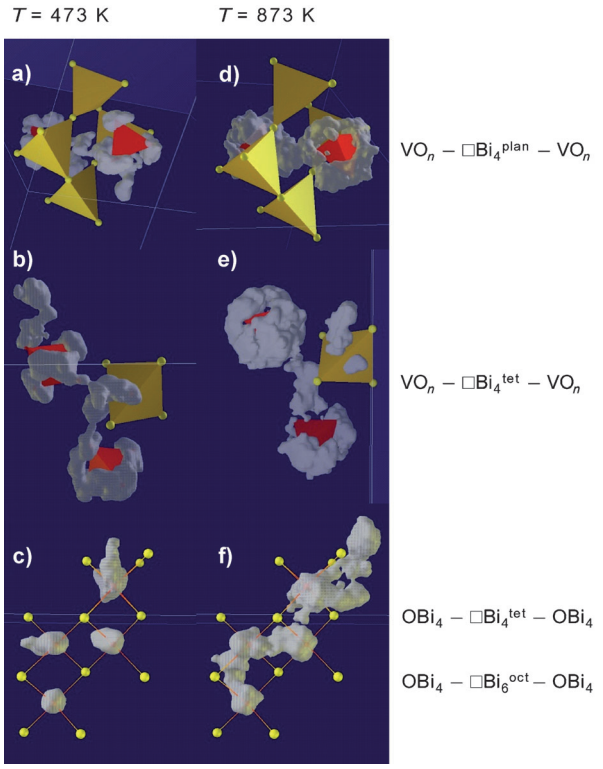

Figure 2. Oxide ion migration pathways obtained by AIMD simulations: a–c) at 473 K; d–f) at 873 K. Vanadium coordination polyhedra shown in red; OBi_4 groups and Bi atoms shown in yellow; displacement clouds shown in white represent regions of space visited by oxide ions.

es. Exchange of oxide ions between the isolated VO_4 tetrahedra, which are around 6.7 Å apart, occurs at both temperatures and proceeds through oxygen atoms passing through a bottleneck/vacancy (□) surrounded by four bismuth atoms in a rhomboidal planar geometry (□Bi_4^{plan}), formed by four corner-sharing OBi_4 tetrahedra (Figure 2a and d). At both temperatures, we also see evidence of O^{2-} diffusion pathways between the two types of structural building blocks, whereby oxide ions migrate from a VO_4 tetrahedron into a vacancy inside a neighboring tetrahedral □Bi_4^{tet} group and onwards to an adjacent VO_4; these exchanges occur through the faces of the □Bi_4 tetrahedra involved (Figure 2b and e). The VO_4 groups are able to rotate, particularly at higher temperature giving, for example, the snowball-like appearance in Figure 2e. The exchange of O^{2-} between the Bi–O sublattice and isolated MoO_4 tetrahedra has also been experimentally observed by ^{17}O NMR spectroscopy in the columnar anionic conductor $Bi_{26}Mo_{10}O_{69}$.[25] Finally, oxygen diffusion through the fluorite-like slabs formed by OBi_4 tetrahedra occurs at 873 K (Figure 2f). Oxide ions from OBi_4 groups can hop into vacancies inside adjacent □Bi_4 tetrahedra directly (through shared edges) or indirectly through intervening octahedral □Bi_6^{oct} sites in the Bi–O sublattice (see Figure S9b and S9c in the Supporting Information); this vacancy hopping mechanism is well-established in δ-Bi_2O_3 based materials.[2] At 473 K, continuous migration pathways between the centers of adjacent tetrahedra are not observed; instead we observe only localized motion in this region of the structure (Figure 2c).

Oxide mean-square displacements (MSDs) were calculated using nMOLDYN, to determine whether the oxygen motion is diffusional or vibrational. Prior to MSD calculations, oxygen atoms were classified as originating from the OBi_4 units or VO_4 units according to their positions in the starting configuration. The MSDs of both types of oxygen obtained in the 873 K simulation (Figure 3a) increase linearly with time, indicating that diffusional motion occurs in both Bi–O and V–O sublattices.

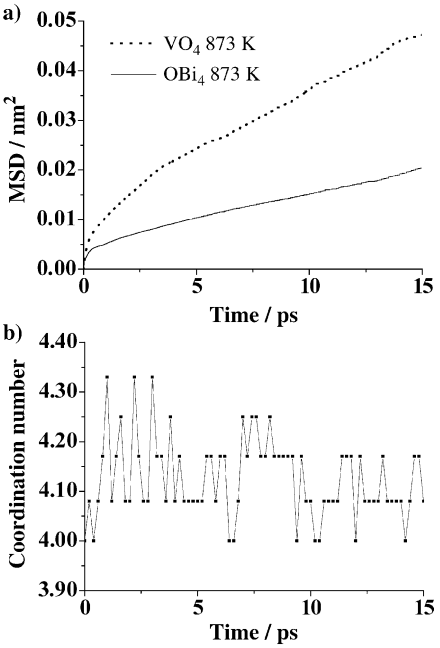

Figure 3. AIMD simulation at 873 K. a) Mean square displacements for oxygen atoms originating from the OBi_4 (solid curve) and the VO_4 units (dotted curve); b) Variation of the average V coordination number during the simulation.

An insight into the role of the V–O sublattice in the oxide ion conductivity of these materials can be obtained by a closer analysis of the V coordination environment during simulations at 873 K (Figure 3b). In this plot, the average coordination number over all 12 V sites is shown as a function of time. The average coordination number during the simulation varies between 4.00 and 4.33; the latter average coordination number corresponds to 4 of the 12 initially tetrahedral V atoms being five-coordinate at any given time (although other combinations are possible, for example, $9+2+1$ or $10+0+2$ four-, five- and six-coordinate V atoms, respectively). This rise in coordination number of vanadium implies creation of additional vacancies in the Bi–O sublattice, which further promotes oxide ion conductivity by vacancy hopping.

Figure 4 illustrates the importance of the variable vanadium coordination environment in oxide ion migration, by showing snapshots of a particular V site at three different steps of the simulation. The change in the coordination number from 4 to 5 to 4 (Figure 4a–c) is facilitated by the

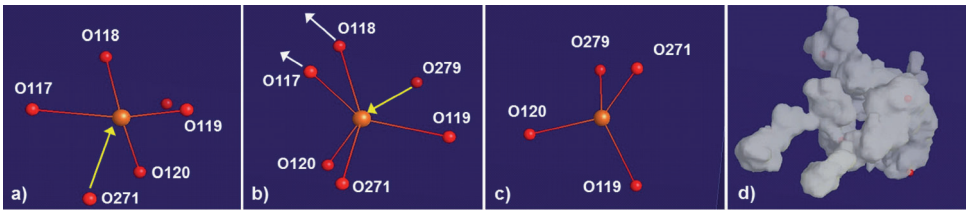

Figure 4. Typical example of variable coordination environment adopted by an individual V atom at three stages of the MD trajectory. a) Four-coordinate V at 3 ps; b) Five-coordinate V at 4 ps; c) Four-coordinate V at 15 ps; d) sum of the O^{2-} displacements around this site. White and yellow arrows show O atoms leaving and entering the V coordination sphere, respectively. Orange spheres show V atoms, red spheres O atoms.

rotation of the VO_n group (manifested as the round white cloud centered on the V atom in Figure 4d); the overall O^{2-} trajectories, which include the oxide ions joining and leaving the coordination sphere as well as the rotation of the coordination polyhedron, are displayed in Figure 4d.

Before concluding on the insights given by AIMD, it is worth briefly revisiting the structural features thought important for high ionic mobility in oxides. Migration in acceptor-doped fluorite-type ionic conductors has long been known to occur through the vacancy hopping mechanism and to be favored by a polarizable cation.[2,26–28] More recently, our structural work correlating the oxygen distribution in $La_2Mo_2O_9$ below and above a crystallographic phase transition which is associated with an increase of oxide ion conductivity of over two orders of magnitude, suggested that the high oxide ion mobility was facilitated by the ability of Mo^{6+} to adopt variable coordination environments.[29] Finally, the rotational flexibility of coordination polyhedra has been found to play an important role for oxide ion conduction mechanisms in structure types containing tetrahedral moieties, such as $La_{1-x}Ba_{1+x}GaO_{4-0.5x}$, cuspidine, apatite,[30,31] and melilite.[32]

We suggest that the remarkably high low-temperature conductivities of $Bi_{0.905}V_{0.095}O_{1.595}$ and $Bi_{0.913}V_{0.087}O_{1.587}$ occur owing to the simultaneous presence of all these advantageous structural features: the highly polarizable Bi–O sublattice containing oxide vacancies (as commonly found in fluorite-based materials); the ability of the V^{5+} cation to adopt variable coordination environments; and the favorable topology of the V–O sublattice, which consists of isolated polyhedra with the V centers 6.7 Å apart, providing sufficient rotational flexibility to support the exchange of oxide ions and sustain their mobility even at moderate temperatures. An additional exceptional feature of our highly conducting materials is that they crystallize as pseudo-cubic long-range ordered fluorite superstructures, leading to increased structural stability and essentially isotropic conductivity and thermal expansion.

In summary, we have shown that $Bi_{0.905}V_{0.095}O_{1.595}$ and $Bi_{0.913}V_{0.087}O_{1.587}$ exhibit remarkably high oxide ion conductivity at low temperatures, comparable to initial measurements on unstable simple cubic δ-Bi_2O_3-based materials and two-dimensional BICUVOX conductors. Conductivity reaches $1.2\times10^{-2}\,S\,cm^{-1}$ at 400 °C, a temperature where we have seen no evidence for sample decomposition. Ab initio MD simulations of the oxide ion migration pathways suggest that the exceptional low-temperature isotropic conductivity in these materials is facilitated by a very high degree of structural flexibility in the solid state, imparted jointly by a highly polarizable sublattice with vacancies, central atoms able to support variable coordination numbers and geometries, and the rotational flexibility of these coordination polyhedra, coexisting in a pseudo-cubic structure. These findings provide generic and widely applicable insight into specific structural features to be sought in future materials discovery efforts aimed at low-temperature oxide ion conductors for energy-related and other applications.

Received: August 29, 2011
Revised: November 11, 2011
Published online: December 1, 2011

Keywords: ab initio calculations · metal oxides · oxide ion conductors · solid-state structures

[1] B. C. H. Steele, A. Heinzel, *Nature* **2001**, *414*, 345–352.
[2] J. B. Goodenough, *Annu. Rev. Mater. Res.* **2003**, *33*, 91–128.
[3] P. Knauth, H. L. Tuller, *J. Am. Ceram. Soc.* **2002**, *85*, 1654–1680.
[4] R. Ramamoorthy, P. K. Dutta, S. A. Akbar, *J. Mater. Sci.* **2003**, *38*, 4271–4282.
[5] A. Lashtabeg, S. J. Skinner, *J. Mater. Chem.* **2006**, *16*, 3161–3170.
[6] D. J. L. Brett, A. Atkinson, N. P. Brandon, S. J. Skinner, *Chem. Soc. Rev.* **2008**, *37*, 1568–1578.
[7] M. Benkaddour, S. Obbade, P. Conflant, M. Drache, *J. Solid State Chem.* **2002**, *163*, 300–307.
[8] R. Punn, A. M. Feteira, D. C. Sinclair, C. Greaves, *J. Am. Chem. Soc.* **2006**, *128*, 15386–15387.
[9] C. H. Hervoches, C. Greaves, *J. Mater. Chem.* **2010**, *20*, 6759–6763.
[10] T. Takahashi, H. Iwahara, *Mater. Res. Bull.* **1978**, *13*, 1447–1453.
[11] H. A. Harwig, *Z. Anorg. Allg. Chem.* **1978**, *444*, 151–166.
[12] V. V. Kharton, F. M. B. Marques, A. Atkinson, *Solid State Ionics* **2004**, *174*, 135–149.
[13] N. X. Jiang, E. D. Wachsman, S. H. Jung, *Solid State Ionics* **2002**, *150*, 347–353.
[14] J. S. Ahn, M. A. Camaratta, D. Pergolesi, K. T. Lee, H. Yoon, B. W. Lee, D. W. Jung, E. Traversa, E. D. Wachsman, *J. Electrochem. Soc.* **2010**, *157*, B376–B382.
[15] J. C. Boivin, C. Pirovano, G. Nowogrocki, G. Mairesse, P. Labrune, G. Lagrange, *Solid State Ionics* **1998**, *113*, 639–651.
[16] G. Mairesse, *C. R. Acad. Sci. Ser. C* **1999**, *2*, 651–660.
[17] A. Watanabe, *Solid State Ionics* **1997**, *96*, 75–81.
[18] Y. D. Li, T. P. Hutchinson, X. J. Kuang, P. R. Slater, M. R. Johnson, I. R. Evans, *Chem. Mater.* **2009**, *21*, 4661–4668.
[19] X. J. Kuang, Y. D. Li, C. D. Ling, R. L. Withers, I. R. Evans, *Chem. Mater.* **2010**, *22*, 4484–4494.
[20] W. Zhou, *J. Solid State Chem.* **1988**, *76*, 290–300.
[21] F. Abraham, J. C. Boivin, G. Mairesse, G. Nowogrocki, *Solid State Ionics* **1990**, *40–1*, 934–937.
[22] T. Takahashi, H. Iwahara, T. Esaka, *J. Electrochem. Soc.* **1977**, *124*, 1563–1569.

[23] O. Turkoglu, I. Belenli, *J. Therm. Anal. Calorim.* **2003**, *73*, 1001 – 1012.
[24] C. I. Thomas, X. J. Kuang, Z. Q. Deng, H. J. Niu, J. B. Claridge, M. J. Rosseinsky, *Chem. Mater.* **2010**, *22*, 2510 – 2516.
[25] L. Holmes, L. M. Peng, I. Heinmaa, L. A. O'Dell, M. E. Smith, R. N. Vannier, C. P. Grey, *Chem. Mater.* **2008**, *20*, 3638 – 3648.
[26] C. R. A. Catlow, *Solid State Ionics* **1984**, *12*, 67 – 73.
[27] J. A. Kilner, *Solid State Ionics* **2000**, *129*, 13 – 23.
[28] S. T. Norberg, S. Hull, I. Ahmed, S. G. Eriksson, D. Marrocchelli, P. A. Madden, P. Li, J. T. S. Irvine, *Chem. Mater.* **2011**, *23*, 1356 – 1364.
[29] I. R. Evans, J. A. K. Howard, J. S. O. Evans, *Chem. Mater.* **2005**, *17*, 4074 – 4077.
[30] E. Kendrick, J. Kendrick, A. Orera, P. Panchmatia, M. S. Islam, A. R. Slater, *Fuel Cells* **2011**, *11*, 38 – 43.
[31] E. Kendrick, J. Kendrick, K. S. Knight, M. S. Islam, P. R. Slater, *Nat. Mater.* **2007**, *6*, 871 – 875.
[32] X. Kuang, M. A. Green, H. Niu, P. Zajdel, C. Dickinson, J. B. Claridge, L. Jantsky, M. J. Rosseinsky, *Nat. Mater.* **2008**, *7*, 498 – 504.

